

Castor oil-based hyperbranched polyurethanes

Highlights

This chapter highlights the synthesis, characterization and property evaluation of castor oil based hyperbranched polyurethane(s) (HPU). HPU was synthesized by using castor oil or its monoglyceride as a biobased B_3 moiety with other reactants such as poly(ϵ -caprolactone)diol as a macroglycol, 1,4-butanediol as a chain extender and toluene diisocyanate by using $A_2 + B_3$ approach. Different spectroscopic and analytical tools were employed to characterize the chemical structure of HPU. The synthesized HPU exhibited good mechanical and thermal properties with excellent chemical resistance in various chemical media. The measurement of dielectric constant and loss factor indicates that HPU behaves as a good dielectric material.

Parts of this chapter are published in

Thakur, S., & Karak, N. Castor oil-based hyperbranched polyurethanes as advanced surface coating materials, *Prog. Org. Coats.* **76**, 157--164, 2013.

2.1. Introduction

From the previous chapter, it is cleared that PU is a versatile polymeric material with a wide range of applicability in diversified fields including coating, adhesive, leather, composite, biomedical, etc.¹⁻³ Various physical and chemical properties of PU can be tuned just by judicious variation of compositions and structures of its three basic building blocks, viz., macroglycol, diisocyanate and chain extender.⁴⁻⁵ These properties of PU can also be tailor-made by physical modification such as blending or through interpenetrating network formation with other polymers.⁶ Thus, proper design of PU with appropriate structure and composition results in unique and useful properties for its avant-garde applications. In this endeavor, hyperbranched PU (HPU) are engraved considerable attention to the researchers over the last two decades. These polymers carved special interest due to their unique architecture and excellent properties like high solubility, low hydrodynamic diameter and low melt as well as solution viscosity.⁷ They exhibit such unusual properties due to their compact, non-entangled and globular structure with large number of active surface functional groups.⁸ Thus, HPU demonstrated better properties compared to its linear analog.⁸ In spite of such advantages of HPU, it suffers from some inadequacy such as inferior mechanical property. This problem is addressed by the incorporation of a long chain containing flexible macroglycol like poly(ϵ -caprolactone)diol (PCL) or poly(tetramethylene oxide) in the structure of HPU.⁹

Again, material scientists made some earnest efforts to develop some alternative feedstocks for the synthesis of HPU due to limited petroleum resources, waste disposal problems and environmental concerns.^{10,11} In this context, the utilization of bio-resources such as vegetable oils as raw materials is good alternative effort for the synthesis of HPU. This is due to numerous advantages of vegetable oils which include easy availability, relatively cost-effective, versatility in structure and property, environmentally benign and most importantly, inherent biodegradability.¹² Different vegetable oils such as castor, canola, palm, linseed, soya bean, coconut, sunflower and *M. ferrea* L. seed oils are used for this purpose.¹²⁻¹⁶ Among the genre of different vegetable oils, castor oil (*R. communis*) is a comparatively inexpensive source of secondary hydroxyl groups and a triglyceride of fatty acids with 92–95% ricinoleic acid (contains a hydroxyl group at 12th carbon on the fatty acid chain).¹⁷ Therefore, it can be used as a bio-resource as well as a multifunctional unit for the synthesis of HPU.

Thus, HPU was synthesized from castor oil and its monoglyceride by using a simple pre-polymerization technique in the present study. The physical and chemical structures of HPU were also characterized by different spectroscopic and analytical techniques. The performance characteristics such as tensile strength, elongation at break, scratch hardness, impact resistance, gloss, chemical resistance in different media, etc. were also investigated and discussed in this chapter.

2.2. Experimental

2.2.1. Materials

Toluene diisocyanate (TDI) (**Table 1.1**, Chapter 1) in a mixture of 80% 2,4- and 20% 2,6-isomers was purchased from Sigma-Aldrich, Germany. Formula weight, density, melting point and boiling point of it are 174.16 g/mol, 1.214 g/cm³, 21.8 °C and 251 °C, respectively. It was used as received as one of the reactants for the synthesis of HPU.

PCL (**Table 1.2**, Chapter 1) was obtained from Solvay Co., UK. Its density, hydroxyl number and number average molecular weight (M_n) are 1.071 g/cm³, 37 mg KOH/g and 3000 g/mol, respectively. It was used after drying under vacuum at 60 °C for 12 h as a macroglycol of HPU.

1,4-butanediol (BD) (**Table 1.3**, Chapter 1) was procured from Merck, Germany. Its density is 1.02 g/cm³ and minimum assay is 99%. It was used as a chain extender after drying under vacuum at 60 °C for 12 h.

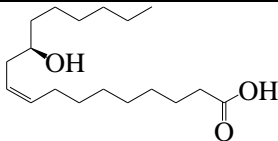
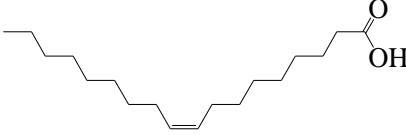
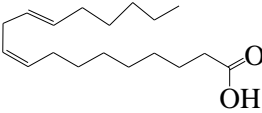
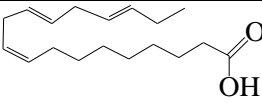
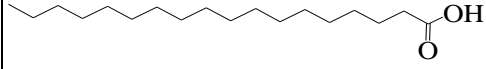
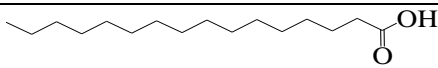
Castor oil was obtained from Sigma-Aldrich, Germany and used after drying in a vacuum oven at 60 °C for 12 h. The composition and structure of the fatty acids of the castor oil are given in **Table 2.1**. It was used as a bio-based triol for HPU.

Glycerol (**Table 1.3**, Chapter 1) was procured from Merck, India. Its purity is 99% and molar mass is 90.09 g/mol. It is a colorless and odorless triol compound. Glycerol is soluble in water and behaves as a hygroscopic viscous liquid. Density, melting and boiling points of it are 1.26 g/cm³, 17.8 °C and 290 °C, respectively. It is used in different pharmaceutical formulations and as a multifunctional moiety in the preparation of hyperbranched polymer. Here, it was used after drying under vacuum at 60 °C for 12 h as a triol (alcoholizing reagent) for converting triglyceride (castor oil) into monoglyceride

Calcium oxide was purchased from S.D. Fine Chemical Ltd., Mumbai. The minimum assay is 95%. Herein, it was used as a catalyst for transesterification reaction of triglyceride with glycerol. It was used as received as base catalyst.

Molecular sieve of 4A type was obtained from Merck, India. It consists of aluminosilicate minerals, clays, porous glasses, microporous charcoals, zeolites, active carbons or synthetic compounds with a porous structure through which small molecules can diffuse. Its equilibrium capacity for water at 30 °C and 75% relative air humidity is $\geq 20\%$ and bulk density is 650-700 g/cm³. It was used as received to trap trace amount of moisture present in solvents.

Table 2.1 Composition and structure of fatty acids of castor oil¹⁸

Name of fatty acid	Structure of fatty acid	Average percentage range
Ricinoleic acid		85 – 95%
Oleic acid		2 – 6%
Linoleic acid		1 – 5%
α -Linolenic acid		0.5 – 1%
Stearic acid		0.5 – 1%
Palmitic acid		0.5 – 1%

Xylene was purchased from Merck, India. It is a colorless liquid with molar mass, density and boiling point of 106.16 g/mol, 0.864 g/cm³ and 138.5 °C, respectively. It was vacuum distilled to use as a solvent and kept in 4A type molecular sieves before use.

Methanol (CH₃OH) was obtained from Merck, India with molar mass 58.0 g/mol, purity $\geq 99.5\%$, density 0.971 g/cm³ and b.p. 56-57 °C. Here, it was used as a solvent.

Sodium chloride (NaCl) crystals, with 99.5% purity were procured from Merck, India. Molar mass and density of NaCl are 58.44 g/mol and 2.16 g/cm³, respectively. NaCl is used for a broad spectrum of industrial purposes such as textiles and dyeing, oil and gas, pulp and paper, leather and rubber manufacturing, etc. Here, its 10% aqueous solution was used as a chemical medium for the chemical resistant test of HPU.

Sodium hydroxide (NaOH) was purchased from Merck, India, with 97% purity. Molar mass of NaOH is 40.0 g/mol. It is used in various industries such as paper, textile, water, detergent, soap, etc., mainly as a strong base. Here, its 10% aqueous solution was used as a chemical medium for the chemical resistant test of HPU.

Hydrochloric acid (HCl) was obtained from Merck, India as 37% (weight by volume) aqueous solution. The molar mass of HCl is 36.5 g/mol. It has various smaller-scale applications, such as household cleaning, production of gelatin and other food additives, descaling, and leather processing. Here, its 5% aqueous solution was used as a chemical medium for the chemical resistant test of HPU.

2.2.2. Characterization

FTIR spectra of HPU were recorded over the wavenumber range of 4000–400 cm^{-1} by a Nicolet FTIR spectrophotometer (Impact-410, Madison, USA) using KBr pellets. The presence of different functional groups in HPU was analyzed by this technique. ^1H NMR and ^{13}C NMR spectra of HPU were taken by FTNMR spectrometer (400 MHz, JEOL, Japan) by using tetramethylsilane (TMS) as an internal standard and d_6 -DMSO as a solvent. UV-spectra of HPU were analyzed in Hitachi (U-2001, Tokyo, Japan) UV spectrophotometer. XRD study was carried out at room temperature (ca. 25 °C) by a Rigaku X-ray diffractometer (Miniflex, UK) over a range of $2\theta=10$ -70°. The thermal analysis, TGA was done by using a PerkinElmer TGA4000 with nitrogen flow rate of 30 mL/min and the heating rate of 10 °C/min from 30 to 700 °C. DSC was carried out by using a DSC 6000 (PerkinElmer, USA) at a heating rate of 2 °C/min under a nitrogen flow of 30 mL/min from -20 to 120 °C by using heating, cooling and heating cycles. The tensile strength and elongation at break of HPU were measured with the help of Universal Testing Machine (UTM, WDW10, Jinan, China) with a 500 N load cell and crosshead speed of 50 mm/min. The polymeric film was placed between the grips of UTM, equipped with an extensometer. For the mechanical test (ASTM D 882), rectangular HPU films were taken with the dimension of $60 \times 10 \times 0.3 \text{ mm}^3$. The scratch hardness of HPU was measured in a scratch hardness tester (Model No. 705, Sheen, UK) associated with a stylus accessory (ASTM G171). Impact strength was tested by the standard falling weight (ball) method (ASTM D 1709) in an Impact tester (S. C. Dey Co. Kolkata, India). In this test, a weight of 850 g is allowed to fall onto HPU film coated on a steel plate from minimum to maximum falling heights. The maximum height was taken as the impact resistance up to which the

film was not damaged. A mandrel with diameter 1-100 mm was used for bending test of HPU films (standard ASTM D 522). The surface morphology was studied by a JEOL SEM of model JSM-6390LV after platinum coating on the surface. The gloss of the films was measured by using a mini-gloss meter (Sheen instrument Ltd., UK). Shear viscosity of the polymers (20% solid content in DMF) was carried out by the help of a rheometer (CVO100, Malvern, UK) with a parallel plate of 20 mm diameter (pp20). The viscosity of the polymer solutions (0.5 g/dL in DMF) was measured at (27±0.1) °C by the help of Ubbelohde capillary viscometer (suspended-level viscometer). The specific gravity of the polymers was evaluated by pycnometer at room temperature (~27 °C) using the conventional liquid displacement method (Archimedes's principle).

The chemical resistance test was performed using the standard ASTM D 543-67 method by taking the weighted amount of film in different chemical media. The test was performed in 250 mL beakers containing 150 mL of the individual chemical medium for the specified period of time. The chemical resistance was determined by measuring the weight changed for the individual film after the completion of the test period. Dielectric properties such as dielectric constant and loss factor of HPU were evaluated by taking thin film of 8 mm diameter (d) and thickness (t) of 0.3 mm, using Hioki-3532-50 LCR Hitester instrument. The measurements were performed at a frequency range of 50-5000 kHz in a symmetric stainless level electrode system at room temperature. The dielectric constant was calculated from the measured values of the capacitance (C_p) obtained directly from the instrument using the following equation.

$$\text{Dielectric constant} = \frac{C_p \cdot t}{\epsilon_0 \cdot A}$$

where ϵ_0 =permittivity of vacuum= 8.85×10^{-12} Farad/m, t=thickness of sample and A=cross-sectional area of the sample= πr^2 , r is the radius of film.

2.2.3. Methods

2.2.3.1. Preparation of monoglyceride of castor oil

The monoglyceride of castor oils was prepared by transesterification reaction.¹⁹ Briefly, a three-neck round bottom flask was equipped with a mechanical stirrer, a thermometer and a nitrogen gas inlet. At first, nitrogen gas was purged into the flask to create inert atmosphere and then, 36.8 g (0.04 mole) of castor oil, 7.36 g (0.08 mole) of glycerol and 0.0184 g (0.05 wt. % with respect to the oil) of calcium oxide were taken into the flask. After that, the mixture was heated up to (225± 5) °C with continuous stirring until it was

transformed to the desired monoglyceride, which was confirmed by its solubility in methanol (monoglyceride:methanol = 1:3, v/ v) at room temperature.

2.2.3.2. Synthesis of HPU

A three-neck round bottom flask equipped with a nitrogen gas inlet, a mechanical stirrer and a rubber septum was used for this polymerization reaction. Required amount of PCL and BD in DMAc were taken in the reaction flask with desired amount of xylene under constant stirring (as BD is insoluble in xylene, so little amount of DMAc was required to dissolve it). After dissolving PCL, the desired amount of TDI was added dropwise into the reaction mixture at room temperature by the help of a syringe through the rubber septum. In this step, NCO/OH ratio was maintained at 0.9 to obtain hydroxyl terminated prepolymer. The reaction was continued for 3 h at (70 ± 2) °C to obtain a viscous mass, which was treated as the pre-polymer.

This pre-polymer was then cooled to room temperature and castor oil or the monoglyceride of the oil as the multifunctional moiety was added with the rest amount of TDI to maintain NCO/OH ratio 1.0. The temperature was then increased again to (110 ± 2) °C and stirred continuously for 2.5 h to complete the reaction as indicated by the absence of isocyanate band at 2270 cm^{-1} in FTIR spectrum.¹⁷ The actual composition of the reactants for both HPUs are given in **Table 2.2**. Castor oil-based and monoglyceride of the oil-based HPU were coded as CHPU and MHPU.

Table 2.2 Composition of the reactants

Reactant	Mol of reactants		Functionality of reactant
	CHBU	MHPU	
PCL	2	2	2
Castor oil	2	0	3
Monoglyceride of castor oil	0	2	3
BD	4	4	2
TDI	9	9	2

Total equivalents of $-\text{OH}=18$

Total equivalents of $-\text{NCO}=18$

2.2.3.3. Sample preparation for performance study

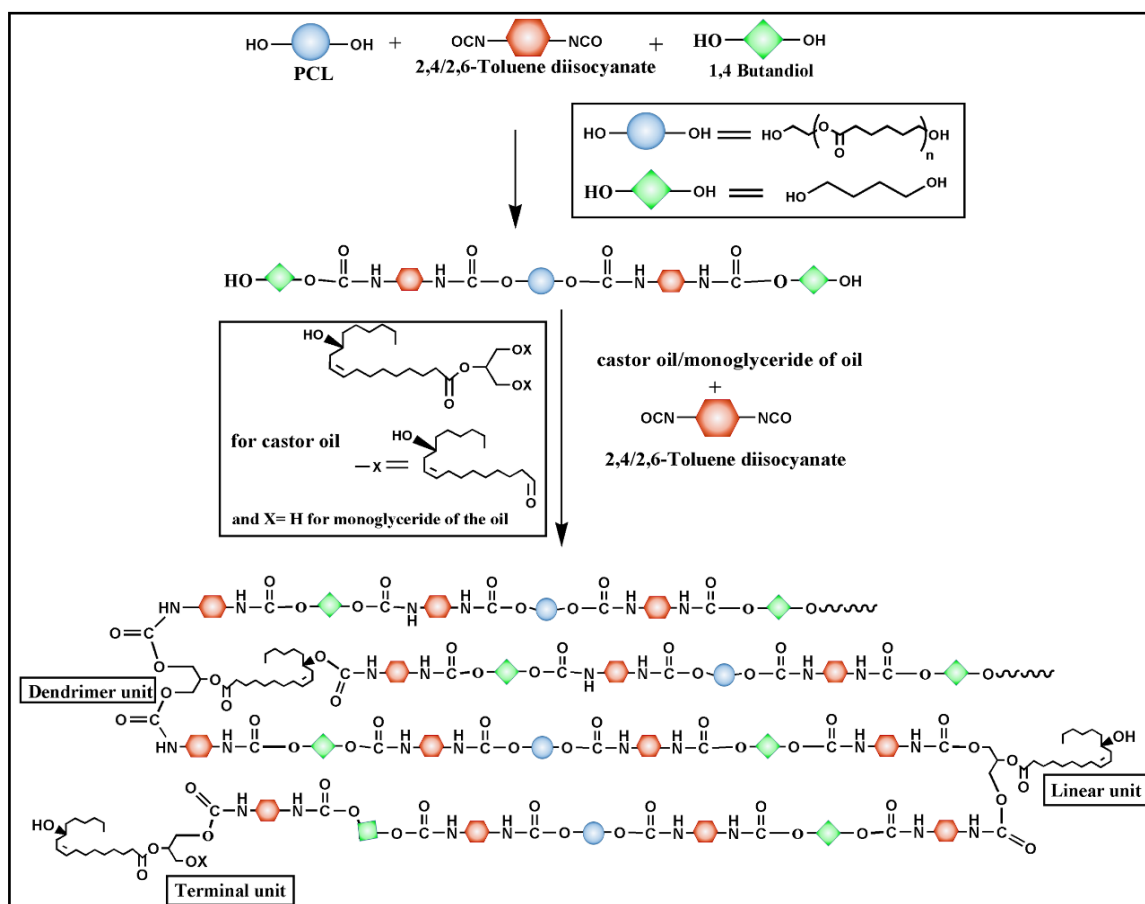
The synthesized HPU was cast on steel plates (150 x 50 x 1.44 mm³) for impact resistance and glass plates (75 x 25 x 1.39 mm³) for gloss, scratch resistance and chemical resistance studies. The coated plates were first allowed to dry under atmospheric pressure followed by degassed under vacuum at 40 °C for 1 h to remove the trace amount of solvent. The dried films from the glass plates were then peeled off by immersing the plates in hot double distilled water, followed by drying under vacuum and stored for 7 days before testing. A small part of the viscous product was precipitated in water and then dried in a vacuum oven at 50 °C for NMR analysis only, whereas all other analyses and testing were performed by using bulk sample without any further purification.

2.3. Results and discussion

2.3.1. Synthesis of HPU

Castor oil and its monoglyceride based HPU with NCO/OH ratio 1.0 were synthesized through a two-step, one-pot, A₂ + B₃ pre-polymerization technique, as shown in **Scheme 2.1**. The hydroxyl terminated pre-polymer was formed in the 1st step of polymerization by the reaction of macroglycol (PCL) and chain extender (BD) with TDI at the required mole ratios (**Table 2.2**). This pre-polymer was used as an A₂ type reactant for the synthesis of HPU. It is pertinent to mention that BD is generally added after the formation of prepolymer in normal cases.¹⁷ In this investigation, both PCL and BD were incorporated together in the 1st step of polymerization and trifunctional castor oil or its monoglyceride was only added in the 2nd step of polymerization. Therefore, the concentration of total di/polyol remains low in the 2nd step and there is no competition among the different hydroxyl reactants. These factors help to prepare HPU without gel formation. As the reactivity of the B₃ moiety (multifunctional moiety, castor oil or its monoglyceride) is less due to the presence of secondary hydroxyl groups, so relatively high temperature is required for the polymerization reaction. Thus, the reaction in the 2nd step was performed by a stepwise increase of the temperature up to 110 °C to complete the reaction. A very dilute solution (15% in xylene) of castor oil or its monoglyceride was added slowly in the 2nd step at room temperature then the temperature was increased slowly up to 110 °C to avoid gel formation. The completion of the reaction was confirmed by the absence of -NCO band at 2270 cm⁻¹ in FTIR spectrum.¹⁷ As the reactivity of the primary hydroxyl group is higher than the secondary hydroxyl group in urethane reaction, so the formation

of MHPU required less time than that of CHPU.²⁰ Polymerization reactions in polyurethane contain the feature of both addition and step-growth polymerization. The reaction mechanism of polyurethane corresponds to a step-growth polymerization but no small molecules are eliminated during polymerization process like addition polymerization. So, it is not a condensation polymerization. The kinetics of polymerization reactions in polyurethane more closely resemble to step-growth polymerization than addition polymerization. Sometimes this kind of polymerization called as rearrangement polymerization.



Scheme 2.1 Synthesis of HPU from castor oil and its monoglyceride

2.3.2. FTIR analysis

FTIR is an important tool to investigate the presence of functional groups and interactions in the structure of HPU. FTIR spectra of CHPU and MHPU are shown in **Figure 2.1**. The absence of a band at $2250\text{--}2270\text{ cm}^{-1}$ suggests the absence of free -NCO group in HPU structure and completion of the reaction. The most important characteristic features of

HPU are the presence of bands at $1060\text{--}1090\text{ cm}^{-1}$ (C–N stretching vibrations), $1140\text{--}1175\text{ cm}^{-1}$ (C–O stretching vibrations), $1557\text{--}1580\text{ cm}^{-1}$ (N–H bending), $1601\text{--}1635\text{ cm}^{-1}$ (C=C stretching vibration), $1710\text{--}1730\text{ cm}^{-1}$ (C=O stretching vibrations from urethane groups), $2859\text{--}2950\text{ cm}^{-1}$ (CH_2 symmetric and anti-symmetric stretching vibrations) and 3430 cm^{-1} (O–H free and N–H stretching from urethane group stretching vibrations).²¹ Thus, the presence of such functional groups suggests the formation of urethane linkage, --NH--C(=O)--O-- in both HPU.²²

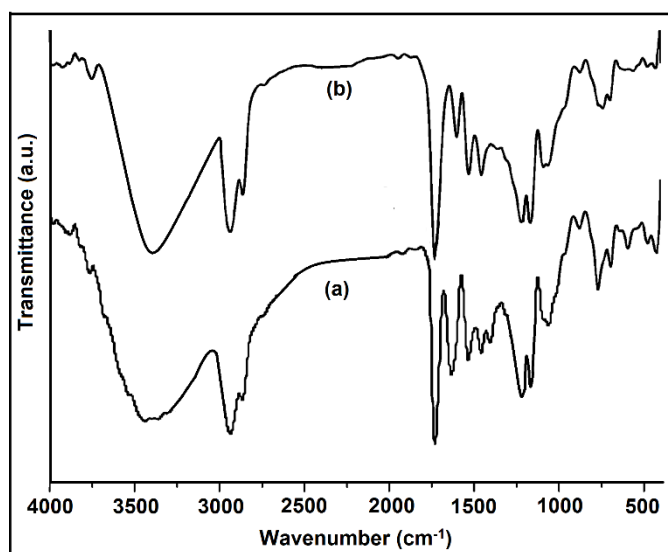


Figure 2.1 FTIR spectra of (a) CHPU and (b) MHPU

2.3.3. NMR study

The structure of HPU was further studied by ^1H and ^{13}C NMR spectroscopy. ^1H and ^{13}C NMR spectra of both HPU (**Figure 2.2** and **2.3**) indicate the presence of urethane linkage, fatty acids moiety of castor oil/monoglyceride, BD, PCL and TDI moieties. In ^1H NMR spectra, peaks at $\delta=0.79\text{--}0.84\text{ ppm}$ and $\delta=1.4\text{--}1.6\text{ ppm}$ are due to the terminal methyl group and protons for $\text{--CH}_2\text{--}$ groups attached next to the terminal methyl group of the fatty acid chain of the oil or its monoglyceride, respectively.²² Protons of allylic $\text{--CH}_2\text{--}$, $\text{--CH}_2\text{--}$ adjacent to the oxygen atom of urethane group and --CH_3 of TDI showed peaks at $\delta=1.93\text{ ppm}$, $\delta=2.2\text{ ppm}$ and $\delta=2.45\text{ ppm}$, respectively.^{22,23} The peaks of --CH attached with --OH linkage and --CH attached with urethane linkage on oxygen side were found at $\delta=3.9\text{ ppm}$ and $\delta=4.03\text{ ppm}$, respectively for HPU. Protons attached to C=C and aromatic protons were appeared at $\delta=5.31\text{ ppm}$ and $\delta=7\text{--}7.6\text{ ppm}$, respectively. Protons attached in the aromatic group between two urethane linkages, adjacent to urethane linkage and

adjacent to methyl group were found at $\delta=7.65$ ppm, $\delta=7.42$ ppm and $\delta=6.99$ ppm, respectively.²³

In ^{13}C NMR, the internal aliphatic carbon peak of the PCL segment appeared at $\delta=28$ ppm (**Figure 2.3**). The smaller peak at $\delta=64$ ppm is associated with soft-segment carbons that are adjacent to a urethane linkage, while the peak at $\delta=70$ ppm is assigned to those soft-segment carbons that are adjacent to oxygen.²⁴ The peak at $\delta=40$ ppm is attributed to methylene carbons of BD, castor oil or monoglyceride. Three different peaks were observed for the aromatic group of TDI at $\delta=127$ ppm, $\delta=129$ ppm and $\delta=132$ ppm for the carbon between two urethane linkages, adjacent to urethane linkage, adjacent to the methyl group, respectively. Peaks were appeared at $\delta=174$ ppm and $\delta=207$ ppm for carbonyl carbon of urethane linkage and ester linkage, respectively.²⁴

Degree of branching of both HPU was determined by a comparison of the integration of the peaks for the substituted and unsubstituted hydroxyl units in HPU from ^1H NMR data as shown in **Figure 2.2**. Degree of branching for CHPU and MHPU were found to be 0.57 and 0.80, respectively.

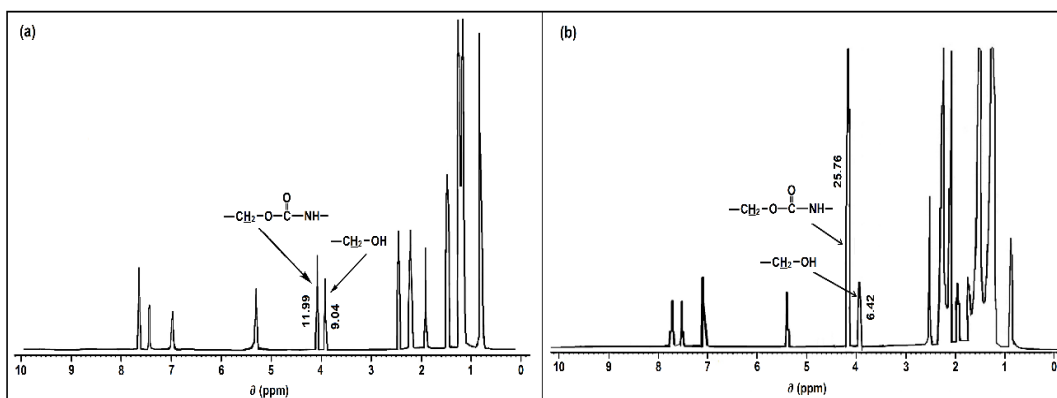


Figure 2.2 ^1H NMR spectra of (a) CHPU and (b) MHPU

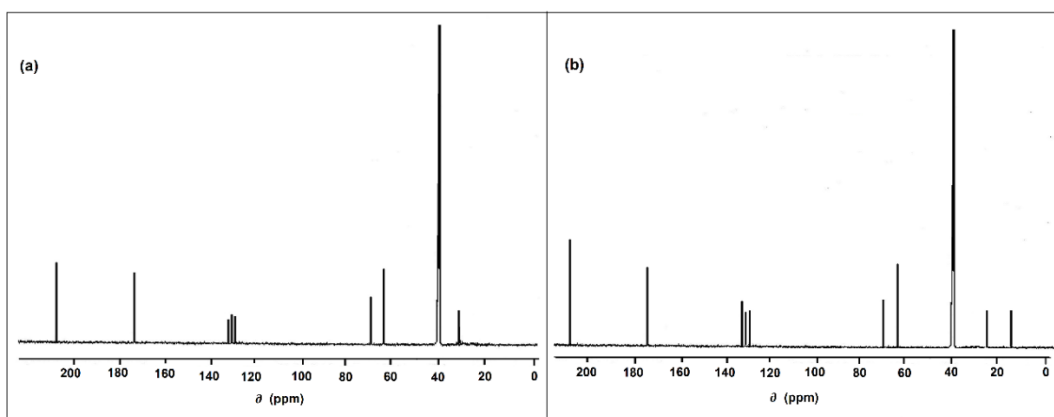


Figure 2.3 ^{13}C NMR spectra of (a) CHPU and (b) MHPU

2.3.4. UV-visible study

The λ_{\max} values were observed at 264 nm and 263.5 nm with low intensity due to $\pi-\pi^*$ transition for C=C presence in the structure of CHPU and MHPU, respectively (**Figure 2.4**). As there was no absorption peak at 286 nm which is the characteristic λ_{\max} for TDI, so it indicates the absence of free TDI in HPU.²²

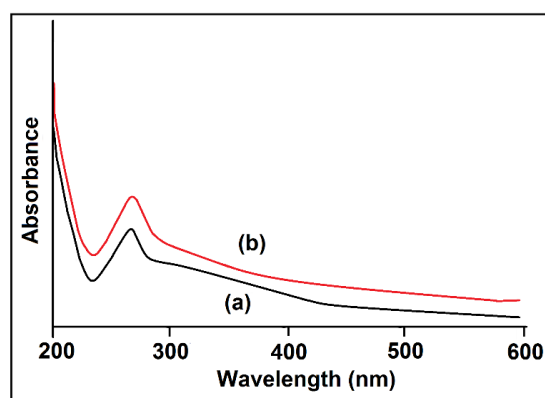


Figure 2.4 UV-visible spectra of (a) MHPU and (b) CHPU

2.3.5. XRD analysis

XRD patterns of HPU are shown in **Figure 2.5**. HPU exhibited basal reflection peaks at $2\theta = 21.6$ (d-spacing = 0.4109 nm) and $2\theta = 23.4$ (d-spacing = 0.379 nm) due to (110) and (200) planes of the PCL crystal.²⁵ The position and nature of the peaks remain same, which indicate that the extent and nature of crystallinity are same for both HPU. Thus, the presence of crystallinity of HPU was confirmed by XRD analysis. The extent of crystallinity was measured and found 28.3% and 26.4% for MHPU and CHPU, respectively. The extent of crystallinity further calculated by DSC study (discussed later).

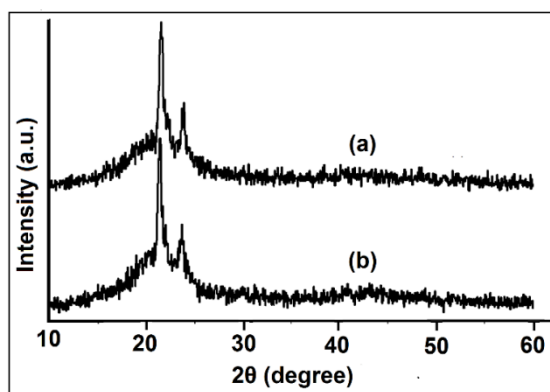


Figure 2.5 XRD patterns of (a) CHPU and (b) MHPU

2.3.6. Morphological study

The morphological study was done with the help of SEM micrographs. SEM micrographs of HPU are shown in **Figure 2.6**. From the micrographs, it is difficult to identify exactly the presence of hard and soft segments though it indicates the uniform phase distribution of HPU.

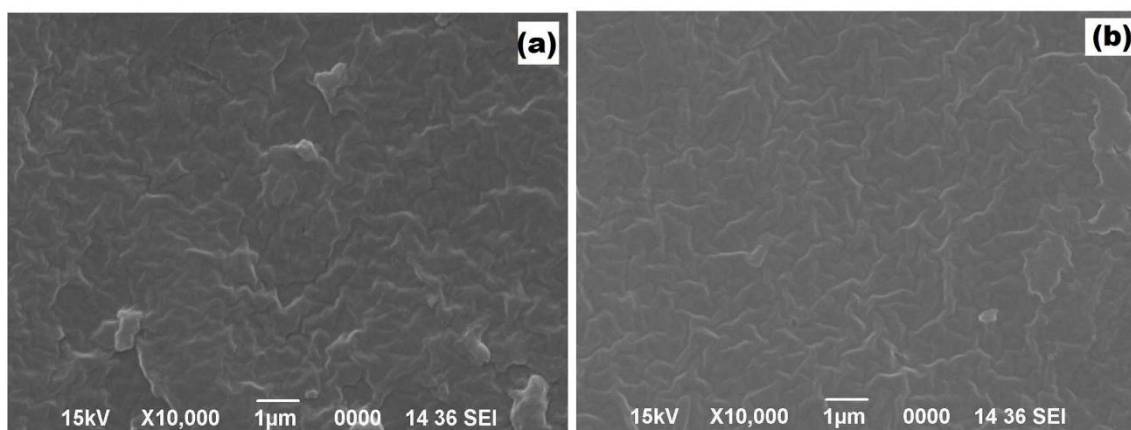


Figure 2.6 SEM micrographs of (a) CHPU and (b) MHPU

2.3.7. Physical properties

One of the most important properties of HPU is the solubility as hyperbranched polymers are well-known for better solubility than their linear analogs. It was found that both HPUs were highly soluble in different polar solvents such as THF, DMF, DMAc, DMSO, etc. The specific gravity of MHPU was found to be slightly higher than CHPU (**Table 2.3**). This might be due to the compact structure of MHPU as supported by the percentage of crystallinity (**Table 2.4**).²² The color of polymer mainly depends on the color of oil or its monoglyceride used for the synthesis of HPU. After casting and drying, both HPU yielded given transparent films. The shear viscosity was slightly higher in CHPU than MHPU, may be due to higher hyperbranched structure of the latter than the former as supported by the degree of branching values (**Table 2.3**).

2.3.8. Thermal properties

The thermal properties of HPU were studied by DSC and TGA. Generally, the thermostability of HPU depends on the number of aromatic moieties and urethane linkages presence in the structure, as they can withstand a considerable amount of heat.¹⁷ The presence of secondary interactions also increases the thermostability of HPU.²⁶ HPU

demonstrated two-step degradation in the TGA thermograms as shown in **Figure 2.7**. The first step is owing to the degradation of the aliphatic chains as well as the breakage of urethane linkages, whereas the second step is due to the degradation of the aromatic moieties.¹⁷

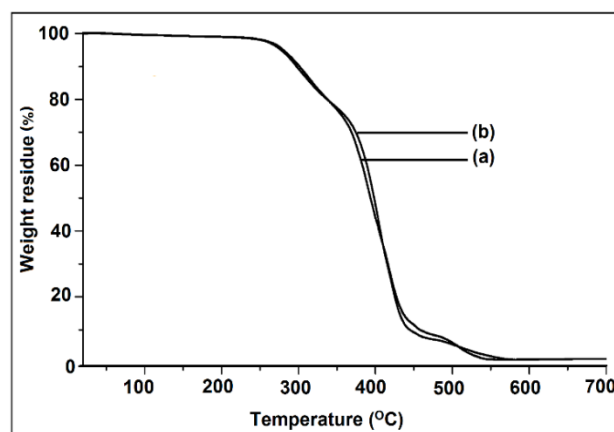


Figure 2.7 TGA thermograms of (a) CHPU and (b) MHPU

Table 2.3 Physical and mechanical properties of HPU

Property	CHPU	MHPU
Color	Transparent off white	Transparent light yellow
Specific gravity	1.06	1.08
Viscosity at 25 °C (Pas)	3.4×10^3	2.1×10^3
Degree of branching	0.57	0.80
Gloss (60°)	74	82
Tensile strength (MPa) ^a	5.8 ± 0.20	7.1 ± 0.30
Tensile modulus (MPa) ^b	2.41 ± 0.24	2.84 ± 0.21
Toughness (MJm ⁻³) ^c	24.63 ± 1.14	25.40 ± 1.28
Elongation at break (%)	791 ± 35	695 ± 30
Scratch hardness (kg)	4.5 ± 0.2	5.0 ± 0.2
Bending test (mm)	<1	<1
Impact test (cm) ^d	>100	>100

^a Defined as the stress at the fracture point. ^b Obtained from the slopes of linear areas in stress–strain curves. ^c Calculated by integrating stress–strain curves. ^dThe limit of the impact strength was 100 cm (highest).

The initial, 50%, and 90% decomposition temperatures, and the weight residue at 500 °C are shown in **Table 2.4**. The initial degradation temperature of MHPU (**Table 2.4**) was found to be higher than that of CHPU. MHPU possesses more compact structure and secondary interactions compared to CHPU.²³ Thus, MHPU exhibited higher thermal stability.

Table 2.4 Thermal properties of HPU

Thermal parameter	CHPU	MHPU
T _{initial} (°C)	259.71	261.2
T _{50%} (°C)	394.2	399.2
T _{90%} (°C)	457.5	445.6
Weight residue at 550 °C (%)	0.9	1.8
Melting temperature (T _m , °C)	48.12	48.79
Crystalline enthalpy (ΔH _c , Jg ⁻¹)	35.21	37.55
Crystallinity (%)	25.88	27.61

DSC curves of CHPU and MHPU are shown in **Figure 2.8**. The crystallization temperature (T_C), melting temperature (T_m) and heat of crystallization (ΔH_C) were obtained from the DSC measurements and summarized in **Table 2.4**.

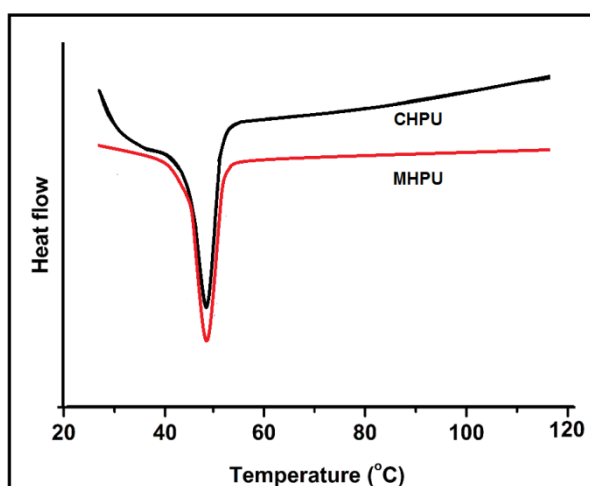


Figure 2.8 DSC curves of CHPU and MHPU

The crystallinity of soft segments in HPU was determined by the measurement of ΔH_C on the cooling cycle and with an enthalpy value of 136 J/g for 100% crystalline PCL. MHPU

exhibited higher T_m than that of CHPU. This may be due to the presence of higher secondary interactions such as H-bonding and polar-polar interactions in MHPU.¹⁷ ΔH_C and percentage of crystallinity were calculated and found higher in MHPU due to high compactness and more aligned structure. Percentage of crystallinity of HPU was found similar trends as found from XRD analysis.

2.3.9. Mechanical properties

The performance characteristics of HPU are given in **Table 2.3**. Both HPU exhibited adequate flexibility as they can be bent in a mandrel with a diameter of 1 mm. This flexibility is attributed to the presence of flexible PCL moiety, ether, ester linkages and the long hydrocarbon chain of the oil in the HPU chains.¹⁷ Mechanical properties of HPU mainly depends on the degree of the urethane groups, physical/chemical cross-linking density and the various interactions such as H-bonding, polar-polar, etc.²⁵ The stress-strain curves for CHPU and MHPU are shown in **Figure 2.9**. The presence of yield and necking points in both the curves indicates the typical elastomeric nature of HPU. MHPU demonstrated higher tensile strength, tensile modulus, toughness and scratch resistance than CHPU. This may be due to the higher crystalline structure of MHPU (**Table 2.4**) and presence of more amount of H-bonding between HPU chains in MHPU which make it hard to stretch.

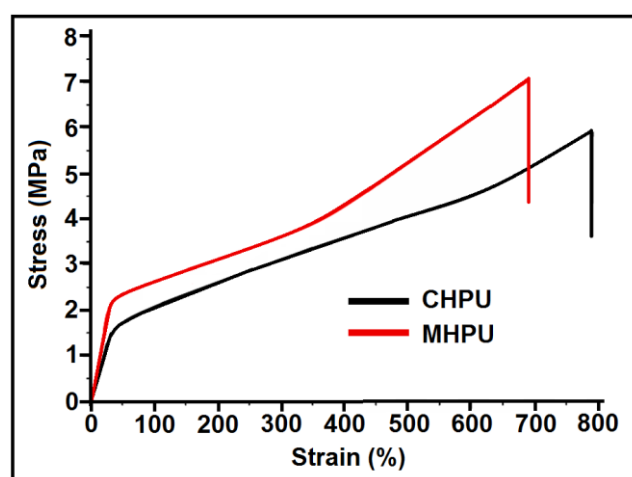


Figure 2.9 Stress-strain profiles of HPU

Both HPU exhibited a lower tensile modulus compared to their tensile strength due to low stiffness and presence of vegetable oil moiety in the structure of both HPU which provides a plasticizing effect.²⁷ Elongation at break was higher for CHPU than MHPU due to the

higher degree of branching in the latter than the formers, which makes a compact structure.²² The impact resistance of both HPU was also very good (>100 cm, 100 cm is a maximum limit of the instrument) owing to their high flexibility and good toughness. The results revealed that MHPU exhibited superior mechanical property than CHPU.

2.3.10. Electrical property

The dielectric constant is the ability of a material to store electric potential energy under the influence of an electric field.²⁸ Variations of dielectric constant with the increase of frequency for HPU are shown in **Figure 2.10**. A constant temperature was maintained during the measurement; hence, its influence on the dielectric constant can be neglected. Dielectric constant is a frequency dependent parameter in polymeric systems.²⁹ It is governed by the number of orientable dipoles present in the polymer chains and their ability to orient under an applied electric field.²⁹

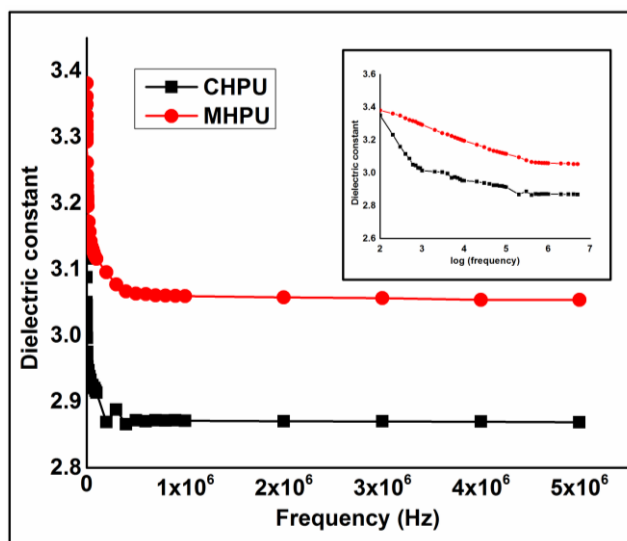


Figure 2.10 Variations of dielectric constant with frequency of CHPU and MHPU (inset shows plot of dielectric constant against log frequency)

A continuous decreased in the dielectric constant was observed upto 500 kHz frequency then it remained almost independent with frequency in both HPU. MHPU showed low dielectric constant than CHPU under the same applied frequency. Usually, the polar functional groups which are attached perpendicular to the longitudinal HPU chain contribute to the dielectric relaxation mechanisms. At lower frequencies of applied voltage, all the free polar functional groups can orient themselves. As a result, HPU

exhibited high dielectric constant value at lower frequencies. The polar groups find difficult to orient at the same speed under the alternating field with increased in the electric field frequency.³⁰ Therefore, the contribution of these polar groups to the dielectric constant reduces continuously. MHPU possesses a compact structure and more secondary interactions such as H-bonding and polar-polar interaction compared to CHPU. These may provide more restriction in MHPU to orient the free polar functional groups. Thus, MHPU showed low dielectric constant than CHPU.

Figure 2.11 illustrates the variation of loss factor with frequency at a constant temperature. In MHPU, the loss factor initially increased at lower frequency then decreased up to a certain frequency and again the pattern was repeated as frequency increased. The first increase of loss factor at lower frequency may be attributed to dipole polarization.²⁷ As the frequency further increases, the dipole polarization effect tends to be zero and thus loss factor tends to very small values. In case of CHPU, loss factor was constant for a long frequency region from 500 to 4000 kHz with a small maximum at 500 kHz was observed. This may be due to small change in polarization and low absorption of moisture, as hydrophobic moiety is predominant in CHPU. A broad maximum of loss factor over the frequency range from 400 kHz to 3500 kHz was observed in MHPU. This may be due to enormous change of polarization and presence of absorbed water molecules in it.²⁷ This suggests that CHPU is more suitable for dielectric material than MHPU as its loss factor is low and remains almost constant over a range of frequencies.³⁰

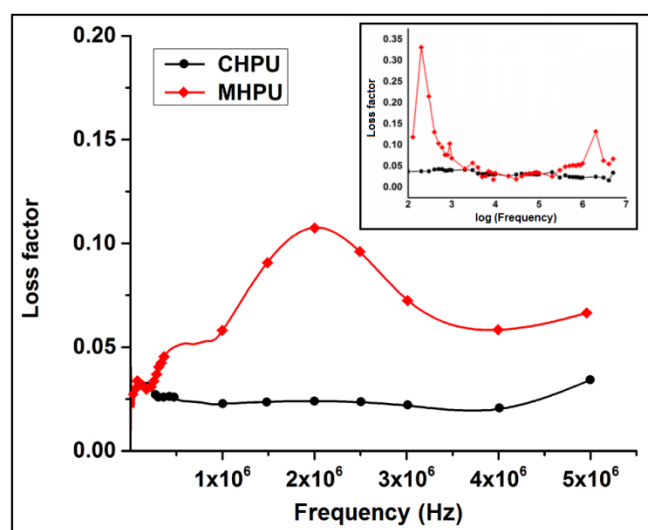


Figure 2.11 Variations of loss factor with frequency of CHPU and MHPU (inset shows plot of loss factor against log frequency)

2.3.11. Chemical resistance

Chemical resistance of HPU was tested in presence of various chemical environments such as 10% aqueous sodium hydroxide (w/v) solution, 10% aqueous sodium chloride (w/v) solution, 5% aqueous hydrochloric acid (v/v) solution and distilled water for 21 days and changes of weights before and after the tests were determined (**Table 2.5**). Both HPU showed very good chemical resistance in all the tested chemical environments. Both HPU have good chemical resistances towards alkali even though it contains hydrolysable ester groups in fatty acid parts. CHPU possesses more hydrolysable ester group owing to the presence of higher amount of hydrophobic fatty acid part but it also showed good alkali resistance. The good chemical resistance of HPU may be due to the high compact structure, presence of secondary interactions such as polar–polar and H-bonding, and presence of aromatic moiety, and so forth.²³

Table 2.5 Changes of wt% of HPU in different chemical media

Polymer	10% aq. NaOH	10% aq. NaCl	5% aq. HCl	Millipore water
CHPU	0.0098	0.002	0.0059	0.002
MHPU	0.0094	0.001	0.001	0.001

2.4. Conclusion

Thus, castor oil and its monoglyceride based HPU were successfully synthesized without gel formation in this study. The synthesized CHPU and MHPU were characterized by different analytical and spectroscopic studies. Degree of branching values were confirmed the formation of hyperbranched structure in the both HPU. CHPU and MHPU demonstrated good thermal properties and chemical resistance toward various chemical media especially the alkali medium. Mechanical properties of MHPU were found better than CHPU due to higher degree of crystalline and compact structure of the former than the latter. Both HPU exhibited frequency dependent dielectric constant at the lower frequency but showed frequency independent behavior at the higher frequency. So, studied HPU possesses potential to be used as thin film materials.

References

1. Guan, J., & Wagner, W.R. Synthesis, characterization and cytocompatibility of polyurethane urea elastomers with designed elastase sensitivity, *Biomacromolecules* **6**, 2833--2842, 2005.
2. Kojio, K., et al. Microphase-separated structure and mechanical properties of norbornane diisocyanate-based polyurethanes, *Polymer* **48**, 997--1004, 2007.
3. Pierce, B.F., et al. Thermoplastic poly(ester urethane)s with novel soft segments, *Macromolecules* **41**, 3866--3873, 2008.
4. Zhang, C., & Feng, S. Effect of glycols on the properties of polyester polyols and of room-temperature-curable casting polyurethanes, *Polym. Int.* **53**, 1936--1940, 2004.
5. Chu, B. et al. Microphase separation kinetics in segmented polyurethanes: Effects of soft segment length and structure, *Macromolecules* **25**, 5724--5729, 1992.
6. Jia, Q.M. et al. Synthesis and characterization of polyurethane/epoxy interpenetrating network nanocomposites with organoclays, *Polym. Bull.* **54** (1-2), 65--73, 2005.
7. Karak, N. & Maiti, S. *Dendrimers and Hyperbranched Polymers--Synthesis to Applications*, MD publication Pvt. Ltd., New Delhi, 2008
8. Voit, B. New developments in hyperbranched polymers, *J Polym. Sci. A Polym. Chem.* **38**, 2505--2525, 2000.
9. Unal, S., et al. A new generation of highly branched polymers: Hyperbranched, segmented poly(urethane urea) elastomers, *Macromolecules* **37**, 7081--7084, 2004.
10. Oprea, S. Synthesis and properties of polyurethane elastomers with castor oil as crosslinker, *J. Am. Oil. Chem. Soc.* **87**, 313--320, 2010.
11. Gunera, F.S., et al. Polymers from triglyceride oils, *Prog. Polym. Sci.* **31**, 633--670, 2006.
12. Sharma, V., & Kundu, P.P. Addition polymers from natural oils-a review, *Prog. Polym. Sci.* **31** (11), 983--1008, 2006.
13. Xu, Y., et al. Morphology and properties of thermoplastic polyurethanes with dangling chains in ricinoleate-based soft segments, *Polymer* **49**, 4248--4258, 2008.
14. Hablot, E., et al. Polyurethanes based on castor oil: Kinetics, chemical, mechanical and thermal properties, *Macromol. Mater. Eng.* **293**, 922--929, 2008.
15. Petrovic, Z.S. Polyurethanes from vegetable oils, *Polym. Rev.* **48**, 109--155, 2008.
16. Javni, I., et al. Effect of different isocyanates on the properties of soy-based polyurethanes, *J. Appl. Polym. Sci.* **88**, 2912--2916, 2003.

17. Karak, N., et al. Synthesis and characterization of castor-oil-modified hyperbranched polyurethanes, *J. Appl. Polym. Sci.* **112**, 736--743, 2009.
18. Sreenivasan, B., et al. Studies on castor oil. I. Fatty acid composition of castor oil, *J. Am. Oil. Chem. Soc.* **33** (2), 61--66, 1956.
19. Dutta, S., & Karak, N. Effect of the NCO/OH ratio on the properties of *Mesua ferrea* L. seed oil-modified polyurethane resins, *Polym. Int.* **55** (1), 49--56, 2006.
20. John, J., et al. Characterization of polyurethane foams from soybean oil, *J. Appl. Polym. Sci.* **86**, 3097--3107, 2002.
21. Jena, K.K., et al. Synthesis and characterization of hyperbranched polyurethane-urea coatings, *Eur. Polym. J.* **43**, 1825--1837, 2007.
22. Deka, H., & Karak, N. Bio-based hyperbranched polyurethanes for surface coating application, *Prog. Org. Coat.* **66** (3), 192--198, 2009.
23. Kalita, H., & Karak, N. *Mesua ferrea* L. seed oil based hyperbranched shape memory polyurethanes: Effect of multifunctional component, *Polym. Eng. Sci.* **52** (11), 2454--2461, 2012.
24. Okamoto, D.T., et al. Carbon-13 NMR investigation of a poly(urethane-urea) system, *Macromolecules* **25**, 1068--1073, 1992.
25. Sahoo, N.G., et al. Effect of functionalized carbon nanotubes on molecular interaction and properties of polyurethane composites, *Macromol. Chem. Phys.* **207**, 1773--1780, 2006.
26. Javni, I., et al. Thermal stability of polyurethanes based on vegetable oils, *J. Appl. Polym. Sci.* **77**, 1723--1734, 2000.
27. Wool, R. & Sun, X.S. *Bio-based Polymers and Composites*, Elsevier Academic Press, Berlington, 2005.
28. Borah, J., et al. Physical, thermal, dielectric and chemical properties of a hyperbranched polyether and its linear analog, *Polym. Degrad. Stab.* **91**, 2911--2916, 2006.
29. Singha, S., & Thomas, M.J. Dielectric properties of epoxy nanocomposites, *IEEE Trans. Dielectr. Electr. Insul.* **15**, 12--23, 2008.
30. Singh, V., et al. Dielectric properties of aluminum-epoxy composites, *J. Appl. Polym. Sci.* **90**, 3602--3608, 2003.

Graphene based HPU nanocomposites as shape memory materials

Highlights

This chapter demonstrates the fabrication of graphene based HPU nanocomposites to obtain shape memory materials with improvement in overall performance for their potential utilization in different advanced fields. The chapter is divided into three sub-chapters, where first sub-chapter describes the preparation, characterization and property evaluation of GO and RGO. Second sub-chapter deals with the fabrication and performance study of HPU/GO nanocomposite. The last sub-chapter demonstrates fabrication and property evaluation of tough RGO based HPU *in situ* nanocomposites using RGO and functionalized RGO (f-RGO) as reactive chain extenders as well as nanoreinforcing materials. The fabricated nanocomposites exhibited improved mechanical and thermal properties. RGO based nanocomposites became conductive upon loading of 2 wt% of nanomaterial. All the nanocomposites showed good shape memory behavior. HPU/f-RGO nanocomposite demonstrated superior shape memory effect, electrical conductivity and mechanical properties than other two types of prepared nanocomposites. These nanocomposites have great potential to be used as smart materials in various advanced applications.

Parts of this chapter are published in

Thakur, S., & Karak, N. Green reduction of graphene oxide by aqueous phytoextracts, *Carbon* **50**, 5331--5339, 2012.

Thakur, S., & Karak, N. Bio-based tough hyperbranched polyurethane-graphene oxide nanocomposites as advanced shape memory materials, *RSC Adv.* **3**, 9476--9482, 2013.

Thakur, S., & Karak, N. Ultratough, ductile, castor oil-based, hyperbranched, polyurethane nanocomposite using functionalized reduced graphene oxide, *ACS Sustainable Chem. Eng.* **2**, 1195--1202, 2014.

Thakur, S., & Karak, N. Multi-stimuli responsive smart elastomeric hyperbranched polyurethane/reduced graphene oxide nanocomposites, *J. Mater. Chem. A* **2**, 14867--14875, 2014.

3A. Reduction of graphene oxide by phytoextract

3A.1. Introduction

Various advantages of castor oil-based HPU are discussed in previous chapter. In spite of such advantages of HPU, it is unable to fulfill the demands of modern advanced applications. All such demands may be satisfied by the formation of nanocomposites with the incorporation of an appropriate nanomaterials as mentioned in Chapter 1. In this context, graphene is one of the most suitable nanomaterials for this purpose to address the challenges of modern avant-garde applications of such polymeric materials.

Graphene, a two dimensional carbonaceous material which is arranged in a layer of carbon atoms packed into a honeycomb structure.¹ It exhibits many inherent unique and fascinating properties such as high Young's modulus (~1TPa), large theoretical specific surface area (2630 m²/g), excellent thermal conductivity (3000–5000 W/mK), high carrier mobility at room temperature (~10,000 cm²/Vs) and good optical transmittance (~97.7%).²⁻⁵ To achieve these properties for different kinds of applications, varieties of synthetic routes are established to prepare graphene such as chemical vapour deposition (CVD), epitaxial growth on electrically insulating surfaces, electric arc discharge of carbon precursors and solution-based chemical reduction of graphene oxide (GO).⁶⁻⁹ Amongst these methods, the solution-based reduction of GO possesses many advantageous features, particularly cost effectiveness and bulk-scale productivity. Despite the distinctive advantages of this method, the reduced GO (RGO) tends to form irreversible aggregation which limits its processability. However, this is eliminated by chemical modification of graphene using small organic molecules, bio-molecules and polymers.¹⁰⁻¹² Another negative aspect of this method is the hazardous nature of the used reducing agents (hydrazine, di-methylhydrazine, hydroquinone, sodium borohydride etc.). To overcome the above problems, a few literature reported on the greener way of reduction of GO using vitamins, alcohols, tea solution, gallic acid, wild carrot root, proteins, bacterial respiration, amino acids, and so forth.¹³ But these green reducing agents also have some shortcomings. In case of wild carrot root, amino acids and vitamin C, high reduction time is required as well as they are expensive material. The tea solution is obtained from an edible item which is not acceptable ethically. Reduction of GO by bacterial respiration also needs special attention and reduction time is quite high. In addition to that, the prepared RGO in all the above cases possesses low electrical conductivity.¹³

Therefore, an effective, low-cost and eco-friendly reducing agent for the chemical synthesis of graphene in mass-scale with high electrical conductivity is highly desirable in most of its applications. From literature, it is cleared that various phytoextracts, obtained from different natural sources like leaves, peels or other parts of plants are usually used as reducing agents for the preparation of different metal nanoparticles like Ag(0) and Au(0).¹⁴ Phytoextract mainly contains various polyphenolic compounds such as catechins, pectins, apigenin, luteolin, ascorbic acid and various flavonoids which showed high tendency to get oxidized.^{15,16} Generally, these types of phytochemicals are readily converted to the corresponding quinone forms in the presence of reactive oxygen species. Thus, the phytoextract possesses sufficient potential to reduce the oxygen containing group of GO.¹⁵ Also, Akhavan et al. reported that antioxidant property of tea polyphenol increased in the presence of iron foil.¹⁷

Thus, in the present sub-chapter, a greener approach was reported for reduction of GO by using aqueous phytoextracts obtained from *Citrus sinensis* peel, leaves of *Colocasia esculenta* and *M. ferrea* Linn, separately. The reduction of GO was also investigated by using aqueous phytoextract in the presence of different metal ions such as Fe³⁺, Cr³⁺, Cu²⁺ and Ni²⁺ under ambient conditions with and without ultrasonication. The obtained RGO was characterized by different analytical and spectroscopic techniques. The electrical conductivity of RGO and reduction mechanism were also delved into.

3A.2. Experimental

3A.2.1. Materials

Graphite flakes (60 mesh, 99% purity) were procured from Loba Chemie, India. Graphite is the most stable allotrope of carbon under ambient conditions. A planar structure arranged in the honeycomb fashion in it. Two common forms of graphite are hexagonal and rhombohedral, both of them are highly thermostable. It is widely used in batteries, lubricants, steel industries, composites, etc. Here, it was used as the precursor for the preparation of GO.

Sulphuric acid (H₂SO₄) was obtained from Merck, India. The molar mass of H₂SO₄ is 98.079 g/mol. It is used as a strong acid in numerous applications including domestic drain cleaner, an electrolyte in lead-acid batteries and various cleaning agents. It is also used as an essential substance in the chemical industry. Here, it was used for the oxidation of graphite.

Potassium permanganate was purchased from Analytical Rasayan, India. It is a strong oxidizing agent and readily dissolves in water to give intensely pink or purple solution. Molar mass, density and melting point of it are 158.034 g/mol, 2.703 g/cm³ and 240 °C, respectively. It was used as an oxidizing agent for the preparation of GO in this study.

Hydrogen peroxide (H₂O₂) was procured from Merck, India. It is a simple form of peroxide and colorless in its neat form. Molecular weight of H₂O₂ is 34.0147 g/mol, melting and boiling points are -0.43 and 150.2 °C. H₂O₂ is a strong oxidizing agent and used as a bleaching agent and disinfectant. It is industrially produced by the hydrolysis of ammonium peroxydisulfate. However, currently, it is manufactured by the reduction of anthraquinone via hydrogenation using palladium catalyst. Anthrahydroquinone undergoes autoxidation, regenerating the starting compound, where H₂O₂ is produced as a by-product. Here, H₂O₂ was used to reduce the residual permanganate and manganese dioxide to colorless water soluble manganese salt.

C. esculenta and *M. ferrea* L. leaves and orange (*C. sinensis*) peels were collected from Tezpur University campus, Assam, India. Phytoextracts of them were prepared separately by stirring 2 g of finely ground leaves or peels in 25 mL of water at 50 °C. Subsequent filtration by a muslin cloth yielded the aqueous phytoextracts. These phytoextracts were used for the reduction of GO.

Ferric chloride anhydrate (FeCl₃), nickel chloride hexahydrate (NiCl₂.6H₂O), chromium chloride hexahydrate (CrCl₃.6H₂O) and copper chloride anhydrate (CuCl₂) were purchased from Merck, India. Molar mass of these salts are 162.2 g/mol, 237.69 g/mol, 266.48 g/mol and 134.45 g/mol for FeCl₃, NiCl₂.6H₂O, CrCl₃.6H₂O and CuCl₂, respectively. These salts were used as a metal ion source for complex formation with phytoextract.

Hydrochloric acid (HCl) was used for washing and removing of excess manganese salt from GO. It was used the same grade as mentioned in Chapter 2, section 2.2.1.

3A.2.2. Characterization

UV-visible, FTIR, TGA and XRD analyses were carried out under the same conditions as stated in Chapter 2, section 2.2.2, by using the same instrumental specifications. An ultrasonicator (UP200S, Hielscher Ultrasonics GmbH, Germany) was used to disperse GO in water, at an amplitude of 60% with 0.5 cycle. Ultrasonicator was operated at a frequency of 24 kHz with standard sonotrode (tip-diameter 3 mm).

Raman spectra of GO and RGO were taken with SPEX 1403 double monochromator coupled to an SPEX 1442. The samples were excited with an air cooled argon ion laser of wavelength 488 nm. The morphology, structure and selected area electron diffraction (SAED) patterns of GO and RGO were analyzed by high resolution transmission electron microscope (HRTEM, JEOL 2100X) at an operating voltage of 200 kV. The electrical conductivity of RGO was measured by using a Keithley 2400 C source meter. The samples for electrical conductivity measurements were prepared by pressing them into pellets of 1 cm diameter. The elemental compositions of GO and RGO were determined by using CHN Analyzer, Model PR 2400 Series II PerkinElmer. The electrochemical properties of RGO were studied using a Sycopel AEW2-10 cyclic voltammeter.

3A.2.3. Preparation of GO

GO was prepared by oxidizing the graphite flakes in a mixture of concentrated sulphuric acid and KMnO_4 according to modified Hummers' method.¹⁸ Briefly, 2 g of graphite powder in 35 mL of 98% H_2SO_4 was taken in a single necked round bottom flask and stirred it on a magnetic stirrer for 2 h. Then, 6 g of KMnO_4 was gradually added into the above solution by maintaining the temperature less than 20 °C using an ice-bath. The mixture was then stirred at 35 °C for 4 h in an oil-bath. The resulting solution was diluted by stepwise addition of 90 mL of water under vigorous stirring and then continued it for 1 h. Then, a dark brown suspension was obtained. The suspension was further treated by adding 30% H_2O_2 solution drop wise until the colour of the solution became bright yellow. The resulting GO suspension was washed by repeated centrifugation, first with 5% aqueous HCl solution to remove excess of manganese salt followed by water until the pH of the solution became neutral. The purified GO was finally dispersed in water (0.5 mg/mL) ultrasonically by using an ultrasonicator.

3A.2.4. Reduction of GO by aqueous phytoextracts

Firstly, 100 mL of GO aqueous dispersion (0.5 mg/mL) was prepared by ultrasonication for 30 min. Then, this dispersion was taken in a single necked round bottom flask and 10 mL of aqueous phytoextract was added slowly into the solution. The resulting suspension was stirred on a magnetic stirrer either at room temperature or under refluxed condition until the reduction was completed (as confirmed by UV analysis). After complete reduction, RGO was settled and it was washed with water for several times to remove the unwanted materials. *C. esculenta* leaf aqueous extract reduced GO, *M. ferrea* L. leaf aqueous extract reduced

GO and *C. sinensis* peel aqueous extract reduced GO were coded as CRGO, MRGO and ORGO, respectively.

3A.2.5. Reduction of GO by aqueous extract of *C. esculenta* in presence of different metal ions

An aqueous phytoextract of *C. esculenta* with different metal ions, separately was added to the GO suspension for the reduction purpose. The prepared GO–metal ion containing *C. esculenta* suspension was stirred at 600 rpm using a magnetic stirrer at room temperature until the color of the solution turned to black from brown. The obtained black precipitate was repeatedly washed with MilliQ water to obtain RGO. A similar method was repeated to reduce the GO suspension under ultrasonication. A constant temperature of 27 °C was maintained during the ultrasonication. *C. esculenta* leaf aqueous extract (in the presence of metal ions) reduced GO was encoded as CMRGO.

3A.3. Results and discussion

3A.3.1. Reduction of GO by phytoextracts

Reduction of GO was carried out by different phytoextracts at room temperature as well as under refluxed condition. In case of *C. esculenta* leaf extract, the reduction was faster than other phytoextracts (*M. ferrea* Linn. leaf and orange peel extracts). Reduction times for all used phytoextracts are given in **Table 3A.1**. It was also observed that the reduction under refluxed condition was much faster than that at room temperature (**Table 3A.1**), as activation energy for the reduction was achieved at a faster rate at the higher temperature. For the reduction, 10 mL of phytoextract was found to be sufficient to reduce 100 mL of GO aqueous dispersion (0.5 mg/mL). Further, it was observed that more amount of phytoextract did not affect the reduction time. Reduction of GO was also studied using *C. esculenta* leaf extract in the presence of different metal ions under ambient conditions with and without ultrasonication. However, the effective reduction was achieved only with Fe³⁺ ions, whereas the reduction efficiency was found to be insignificant for other metal ions (Cr³⁺, Cu²⁺ and Ni²⁺). The reduction in the presence of Fe³⁺ was ultrafast. It took only 3 min though 8 min was required without ultrasonication (**Table 3A.1**). This is a significant achievement as 8 h was required to reduce GO at room temperature when *C. esculenta* aqueous extract was used without metal ions. On completion of the reduction process, the color was changed from

brown to black with simultaneous precipitation of the reduced product. This suggests that oxygen-containing moieties present in GO might be removed.¹⁰

Table 3A.1 Time taken by different phytoextracts for reduction of GO

Phytoextract	At room temperature (h)	Under refluxed (h)
<i>C. esculenta</i> leaf aqueous extract	8	5
<i>M. ferrea</i> Linn. leaf aqueous extract	10	8
<i>C. sinensis</i> peel aqueous extract	10	8
<i>C. esculenta</i> leaf aqueous extract + Fe ³⁺ ions	3 min (under ultrasonication)	–
	8 min (without ultrasonication)	–

3A.3.2. UV- visible absorption study

The reduction reaction was monitored by recording the UV–visible absorption spectra of RGO as a function of time. GO showed a maximum absorption peak at 232 nm and a weak shoulder at 300 nm. These peaks are attributed to the π - π^* transitions of the aromatic C=C bonds and n- π^* transitions of C=O bonds, respectively.¹⁶ After complete reduction, a red shift of the maximum absorption peak was observed at 271 nm for CRGO, at 270.5 nm for CMRGO, at 268 nm for both MRGO and ORGO. This indicates that the electronic conjugation is restored after reduction (**Figure 3A.1**).¹⁶

3A.3.3. FTIR study

FTIR spectra of graphite, GO, CRGO, CMRGO, MRGO and ORGO are shown in **Figure 3A.2**. The appearance of intense bands at 1720 cm⁻¹ (for C=O stretching), 1204 cm⁻¹ (for C–O–C stretching), 1049 cm⁻¹ (for C–O stretching) and a broad band at around 3400 cm⁻¹ for hydroxyl group indicates the presence of oxygen containing moieties such as carbonyl, carboxylic, epoxy and hydroxyl in GO.¹⁹ The removal of such oxygen-containing groups of GO in all RGO are clearly indicated by disappearance of C=O stretching, C–O–C stretching, C–O stretching bands and relative diminution in the intensity of the broad band at 3400 cm⁻¹ for the hydroxyl group. From these spectra of RGO, it is cleared that the used phytoextracts showed strong potential to reduce GO.

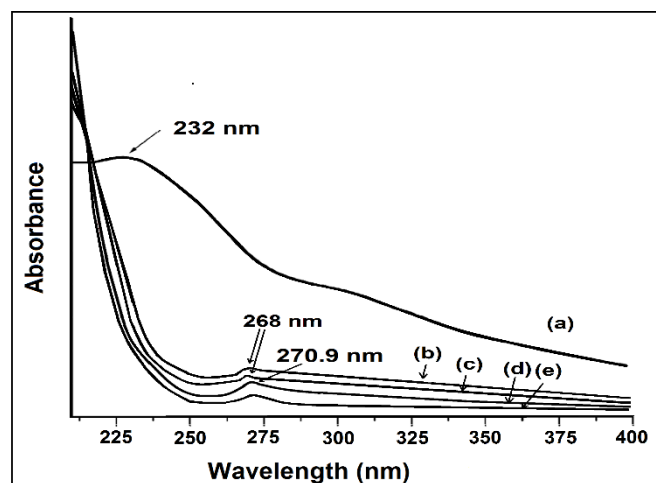


Figure 3A.1 UV-visible spectra of (a) GO, (b) ORGO, (c) MRGO, (d) CRGO and (e) CMRGO

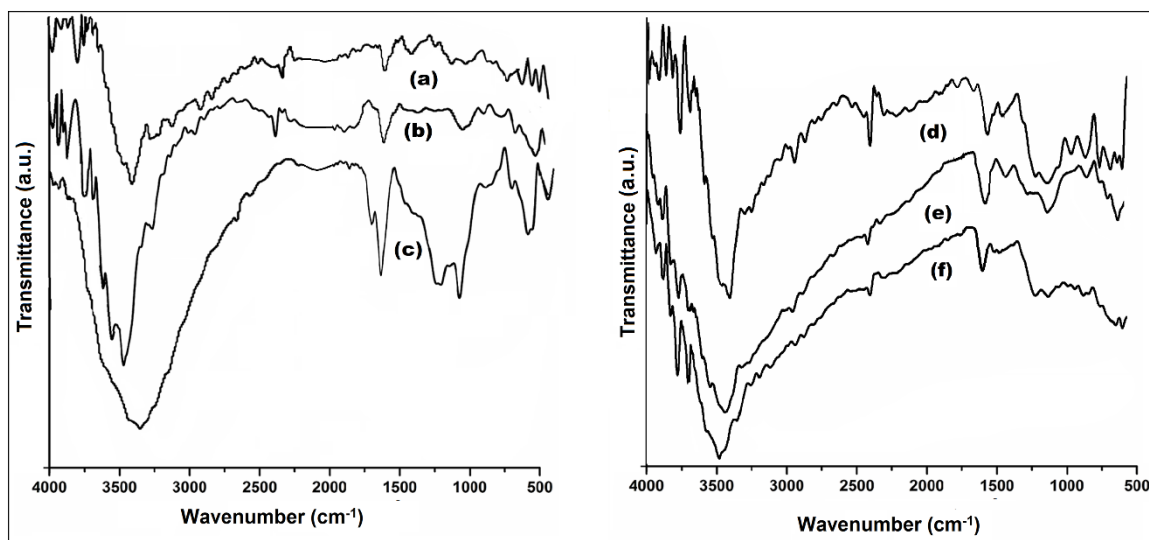


Figure 3A.2 FTIR spectra of (a) graphite, (b) CRGO, (c) GO, (d) MRGO, (e) ORGO and (f) CMRGO

3A.3.4. XRD study

XRD patterns of graphite, GO, CRGO, CMRGO, MRGO and ORGO are shown in **Figure 3A.3**. Pristine graphite demonstrated a basal (002) peak at $2\theta = 26.6^\circ$ corresponding to d-spacing of 0.335 nm.¹⁹ Upon oxidation of pristine graphite, the (002) peak shifts to the lower angle at $2\theta = 9.75^\circ$, (d-spacing = 0.906 nm). The increased in d-spacing is due to the intercalation of water molecules and the formation of oxygen containing functional groups between the layers of the graphite.²⁰ In contrast to GO, all RGO showed a broad peak centred at $2\theta = 25^\circ$ corresponding to d-spacing of 0.36 nm which may be due to restacking of

graphene layers. The close d-spacing of RGO to pristine graphite and disappearance of the peak at $2\theta = 9.75^\circ$ indicated that the oxygen containing group of GO were efficiently removed. In both GO and all the RGO, a less intense peak at 43° was observed due to (100) plane of graphene.²¹ In graphite, a small peak at 53° was observed for (004) plane along with (002) plane.²²

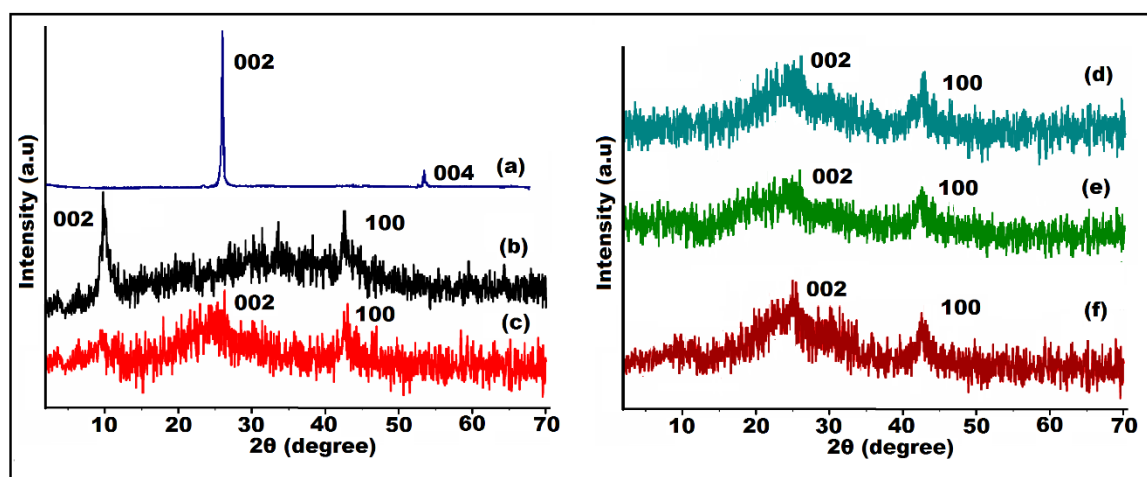


Figure 3A.3 XRD patterns of (a) graphite, (b) GO, (c) CRGO, (d) MRGO, (e) ORGO and (f) CMRGO

3A.3.5. Raman study

Raman scattering is a useful tool to characterize graphite and graphene materials as mentioned in Chapter 1. Raman spectrum of GO was found to be significantly changed after the reduction (**Figure 3A.4**). In the spectra of GO and RGO, two fundamental vibration bands (D and G band) were observed in the range of 1100 to 1700 cm^{-1} . The G vibration mode, owing to the first-order scattering of E_{2g} phonons by sp^2 carbon of GO and RGO were found 1587 and 1584 cm^{-1} respectively, while the D vibration band obtained from a breathing mode of κ -point photons of A_{1g} symmetry of GO and RGO appeared at 1322 and 1327 cm^{-1} respectively.¹⁹ After reduction of GO, the intensity ratio of the D band to the G band (I_D/I_G) was increased significantly. As D band arises due to sp^2 carbon cluster, higher intensity of D band suggested the presence of more isolated graphene domain in RGO compare to GO and removal of oxygen moieties from the former.^{16,23} It is well known that the two-phonon (2D) Raman scattering of graphene-based materials is a valuable band to differentiate the monolayer graphene from double-layer/multi-layer graphene as it is highly perceptive to stacking of graphene layers.²³ Generally, a Lorentzian peak for the 2D band of

the monolayer graphene sheets is observed at 2679 cm^{-1} whereas this peak is broadened and shifted to higher wavenumber in case of the multi-layer graphene.²³ In this investigation, 2D bands were observed at 2696 and 2709 cm^{-1} for GO and RGO, respectively. This indicates that both GO and RGO possess multilayer structure. It is also cleared that the 2D band was shifted toward higher value after reduction of GO which suggested about stacking of graphene layers.²³ As, GO has different types of functional groups which may prevent stacking of graphene layers but after reduction due to a decrease of such functional groups a few graphene layers are stacking and formed multilayer RGO.

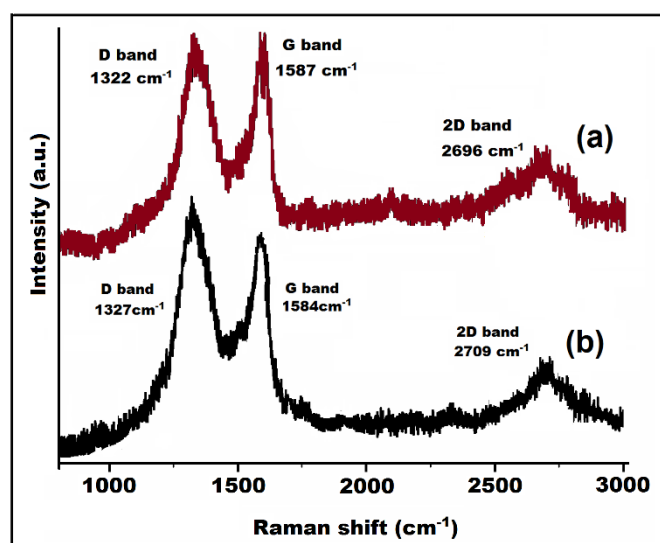


Figure 3A.4 Raman spectra of (a) GO and (b) CRGO

3A.3.6. HRTEM analysis

HRTEM micrographs of GO and RGO are shown in **Figure 3A.5**. **Figure 3A.5a** shows a silk like appearance of GO. Further, from **Figure 3A.5b**, it is cleared that RGO platelet is almost 5.3 nm thick and consisting of 14 layers. So, the interlayer distance is almost 0.37 nm which is in agreement with the XRD result. **Figure 3A.5d** displays a crumpled morphology of CMRGO and the SAED pattern (in the inset) shows a typical semicrystalline ring composed of many diffraction spots, indicating the loss of long range ordering like graphitic structure in RGO.

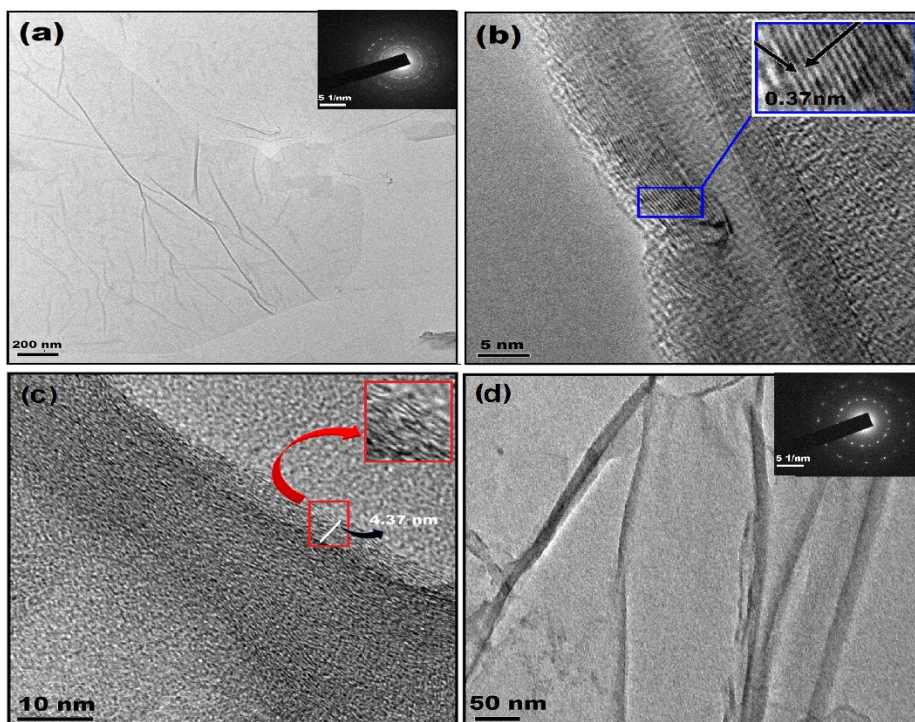


Figure 3A.5 HRTEM images of (a) GO, (b) CRGO showing layer structure, (c) CMRGO showing layer structure and (d) CMRGO showing the sheet like morphology (Inset shows the corresponding SAED pattern)

3A.3.7. Thermal study

Thermal stability of GO, CMRGO, CRGO, MRGO and ORGO were examined by TGA (**Figure 3A.6**). GO and RGO showed no significant weight loss near 100 °C, as the samples were completely dried before testing to eliminate the influence of absorbed moisture on the test results. GO exhibited two steps degradation.

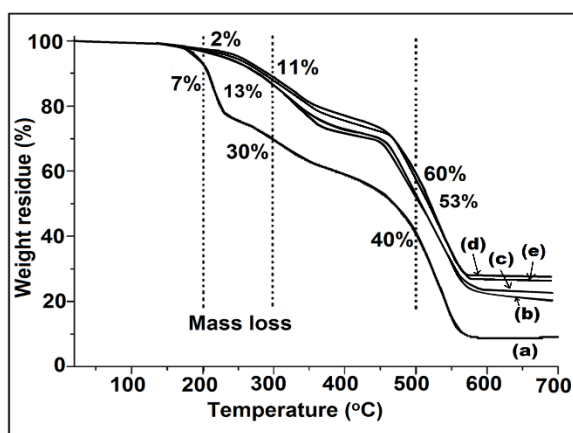


Figure 3A.6 TGA thermograms of (a) GO, (b) ORGO, (c) MRGO, (d) CRGO and (e) CMRGO

The first step of degradation was started at 175 °C due to the loss of hydroxyl, epoxy functional groups and remaining water molecules.¹⁶ The second step degradation (450–550 °C) involves the pyrolysis of the remaining oxygen-containing groups as well as the burning of ring carbon.¹⁹ RGO exhibited only a 7-9 wt% loss up to 250 °C, which was much lower than that of GO. This indicates a significantly decreased in the amount of oxygenated functional groups after reduction. RGO experiences 20% less weight loss in the 1st step of degradation than GO which is also an indication of the degree of reduction.²⁴

3A.3.8. Elemental analysis and electrical study

Elemental compositions of GO and RGO were determined by elemental analysis. Carbon to oxygen ratio (C/O) of CRGO, CMRGO, MRGO, ORGO and GO were found to be 7.11, 6.34, 6.09, 5.97 and 2.68 respectively which further support the efficient reduction by phytochemicals. Generally, the extent of reduction and the restoration of electronic conjugation were also reflected by electrical conductivity of RGO.²⁵ Electrical conductivity of a thin circular RGO pallet (1 cm diameter with 1 mm thickness) was measured by a four-probe setup. The average conductivity of RGO was found to be $4006 \pm 184 \text{ Sm}^{-1}$, $3758 \pm 162 \text{ Sm}^{-1}$, $3184.5 \pm 162 \text{ Sm}^{-1}$ and $3032.6 \pm 157 \text{ Sm}^{-1}$ for CRGO, CMRGO, MRGO and ORGO, respectively. These values are almost 10^4 times higher than that of GO (**Figure 3A.7**).

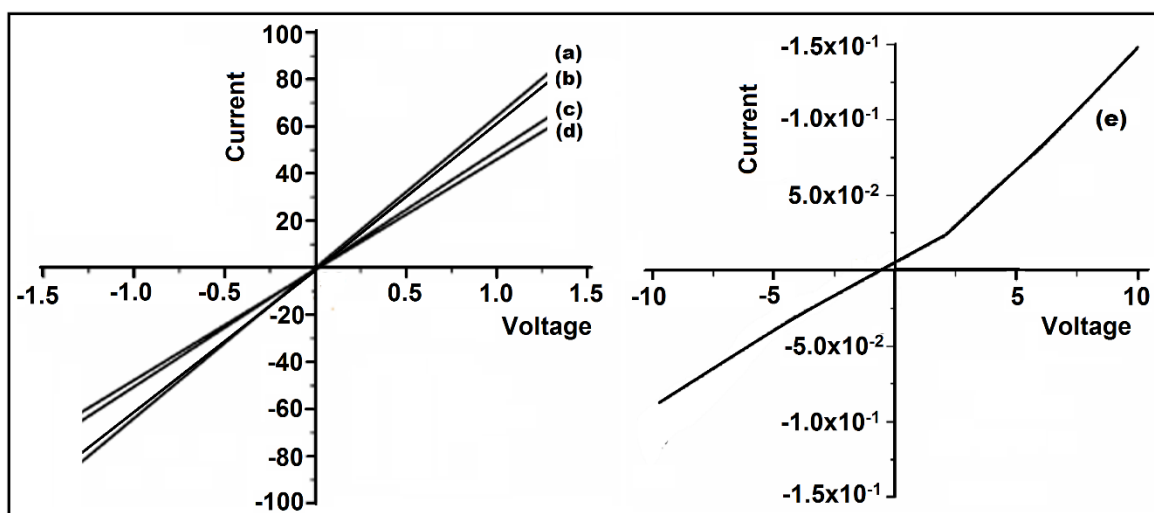


Figure 3A.7 I-V curves for (a) CRGO, (b) CMRGO, (c) ORGO, (d) MRGO and (e) GO

This result clearly indicates the regaining of the electronic conjugation and efficiency of phytoextracts on the reduction of GO. The linear behavior of the current-voltage curves of

RGO suggests the metallic nature of the sheets and formation of Ohmic contact between the sheets and the electrodes.²⁶

The band gaps of GO and RGO were calculated from UV-visible spectra using the following equation²⁷

$$\alpha = \frac{C (h\nu - E_{bulk})^{1/2}}{h\nu} \text{----- (3A.1)}$$

where α is absorption coefficient, C is a constant, $h\nu$ is the photon energy and E_{bulk} is bulk 'band gap'. The band gaps were obtained from the extrapolation of a linear regression to $(\alpha h\nu)^2 = 0$ in the plot of $h\nu$ versus $(\alpha h\nu)^2$ in **Figure 3A.8**. The band gaps of CRGO, MRGO, ORGO and GO were found to be 3.65, 3.62, 3.60 and 4.3eV, respectively. The obtained band gaps are in agreement with the previously reported values.²⁸

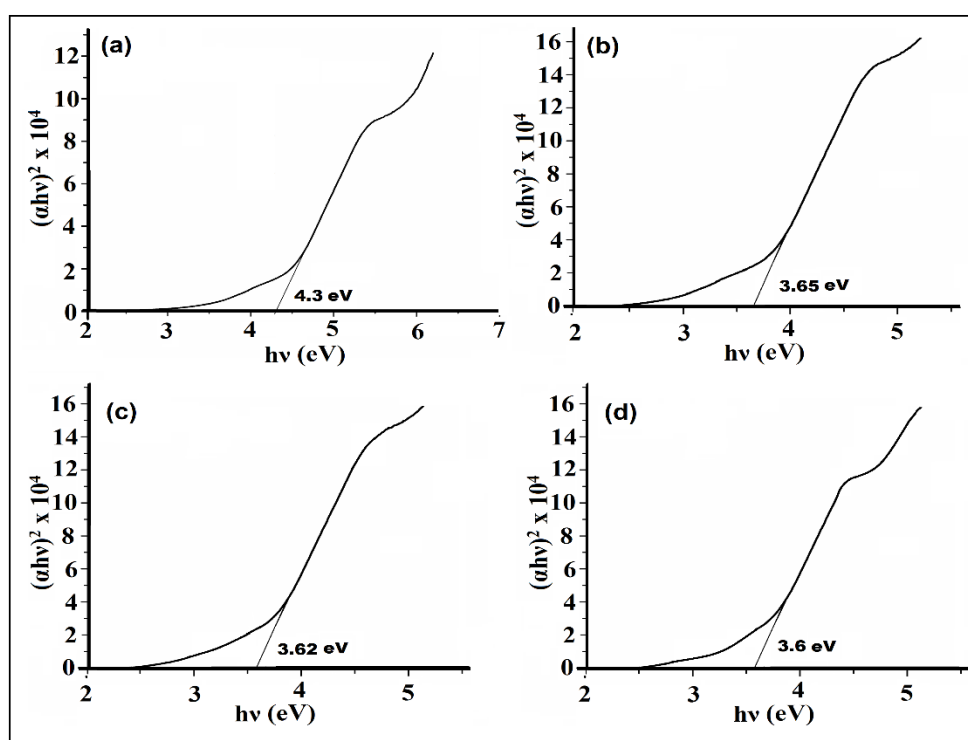


Figure 3A.8 (i) Plots of $(\alpha h\nu)^2$ vs $h\nu$ for (a) GO, (b) ORGO, (c) MRGO and (d) CRGO

The specific capacitance of CRGO, MRGO and ORGO was measured with a cyclic voltammeter where Pt black, Ag/AgCl, and Pt wire were used as the working electrode, the reference electrode and the counter electrode, respectively using a 0.1 M KCl/acetonitrile solution as a supporting electrolyte. Typical rectangular shaped voltammetric profiles were obtained and the average specific capacitances were found to be $21(\pm 2) \text{ Fg}^{-1}$ for ORGO, $18(\pm 2) \text{ Fg}^{-1}$ for MRGO and $17(\pm 1.5) \text{ Fg}^{-1}$ for CRGO (**Figure 3A.9**).

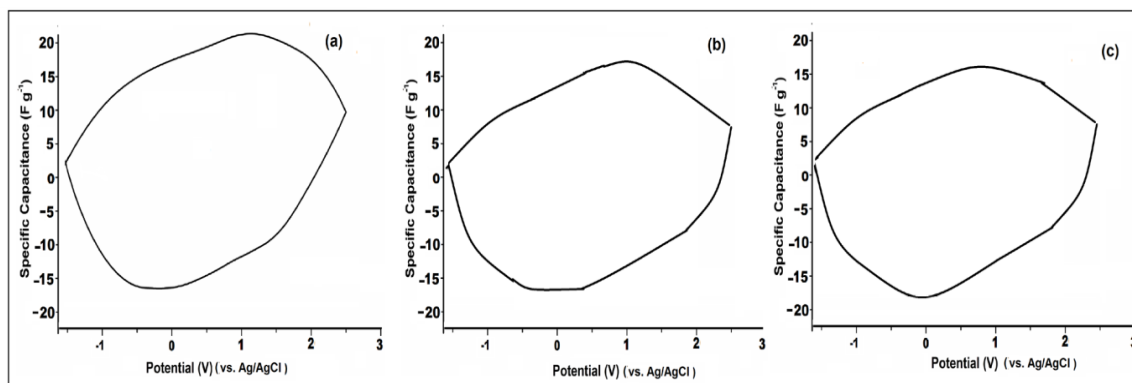


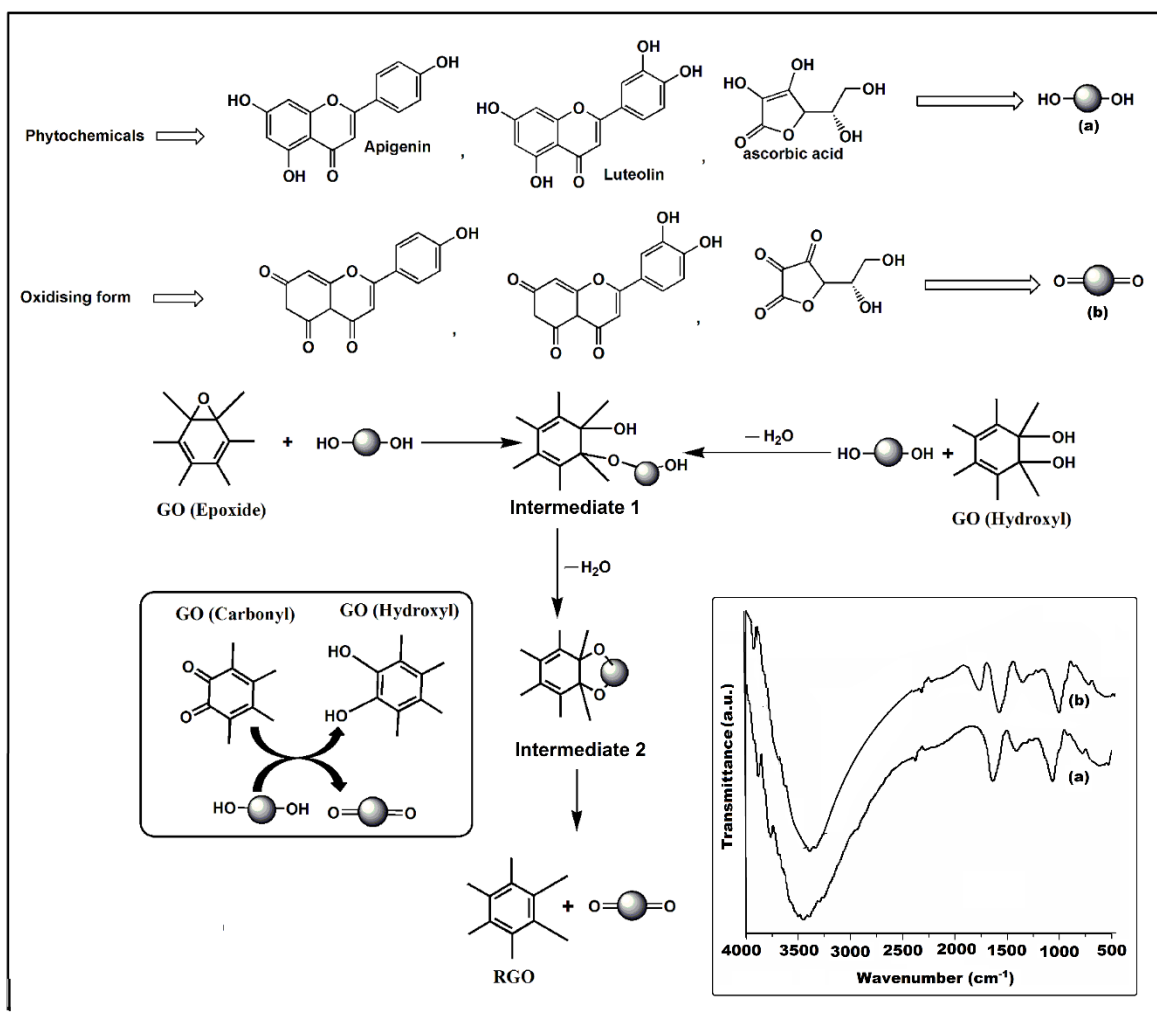
Figure 3A.9 Variation of specific capacitance against potential for (a) ORGO, (b) MRGO and (c) CRGO

3A.3.9. Proposed mechanism of reduction of GO by phytoextract

The proposed mechanism for the reduction of GO is shown in **Scheme 3A.1**. It is supposed that the hydroxyl groups of polyphenol (PP) are highly acidic due to electron withdrawing effect of 5/6-membered PP rings.²⁹ As a result, the proton is readily dissociated from PP and thus it acts as a nucleophile. GO mainly contains three types of reactive species namely epoxide, hydroxyl and carbonyl. The oxygen anion of PP reacts with the epoxide moiety through a SN^2 mechanism resulting in the opening of the oxirane ring of the latter (to form intermediate 1).²⁹ The carbonyl and hydroxyl groups experience similar nucleophilic attack by the oxygen anion of PP. The intermediate 1 transformed to intermediate 2 which finally undergoes elimination reaction to yield RGO. To verify the proposed reaction mechanism, FTIR spectra of *C. esculenta* leaf extract and its oxidising form (collected from reaction medium after the reduction and dried in vacuum oven) were taken and shown in **Scheme 3A.1** (inset). The absence (inset FTIR spectrum a) and the presence (inset FTIR spectra b) of carbonyl band clearly support that the reaction proceed through the described path.

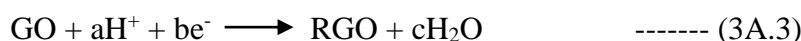
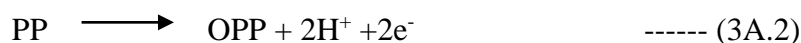
The attenuation of the reduction time (in metal ions containing phytoextract) simply suggests the effective improvement of reduction ability of phytoextract in the presence of metal ions (Fe^{3+}). This results in a quick reduction of GO. As Fe^{3+} can form a stable and stronger complex compared to other studied metal ions with PP which presents in the phytoextract, so faster reduction of GO was achieved.¹⁷ During the complexation process, high amount of H^+ ions was released which changed the pH of the system. The pH values of phytoextract and metal ion containing phytoextract were measured and found to be 6.03 and 3.21 respectively. In order to understand the effect pH, a reduction was carried out by adjusting the pH of the mixed suspension at 3.2, but the same extent of reduction did not

achieve even after 1 h. This suggests that pH has no effective influence on reduction process.



Scheme 3A.1 Proposed reaction mechanism for the chemical reduction of GO by phytoextracts

It was reported that ultrafast reduction was achieved by increasing the reduction potential difference between the two systems.²¹ The reduction of GO with metals containing PP includes two half chemical reactions as shown below.



where OPP is oxidized form of PP and a, b and c are numerical values. The corresponding electrode potential equations can be written as shown below.

$$E_{\text{mC}} = E_{\text{mC}}^{\circ} - \frac{RT}{2F} \ln \frac{1}{[\text{OPP}][\text{H}^+]^2} \quad \text{----- (3A.4)}$$

$$E_{\text{GO}} = E_{\text{GO}}^{\circ} - \frac{RT}{bF} \ln \frac{1}{[\text{H}^+]} = E_{\text{GO}}^{\circ} - 2.303 \frac{RT}{bF} \text{pH} \quad \text{----- (3A.5)}$$

where E_{mC}^0 and E_{GO}^0 are the standard reduction potential of *C. esculenta* aqueous extract in the presence of Fe^{3+} and GO.

To confirm the role of reduction potential, the reduction potential values of GO (E_{GO}) at pH 6.0 and 3.2, *C. esculenta* aqueous extract (E_C) and *C. esculenta* aqueous extract in presence of Fe^{3+} ions (E_{mC}) were measured. The values of $E_{GO(6)}$, $E_{GO(3.2)}$, E_C and E_{mC} were found to be -0.6V, -0.21V, -1.6 V and -1.4 V respectively using Ag/AgCl as the reference electrode (**Figure 3A.10**). As E_{mC} mainly depends on the concentration of H^+ ion, E_{mC} found to be higher than E_C . Even though the concentration of free OPP decreased due to the complexation process.

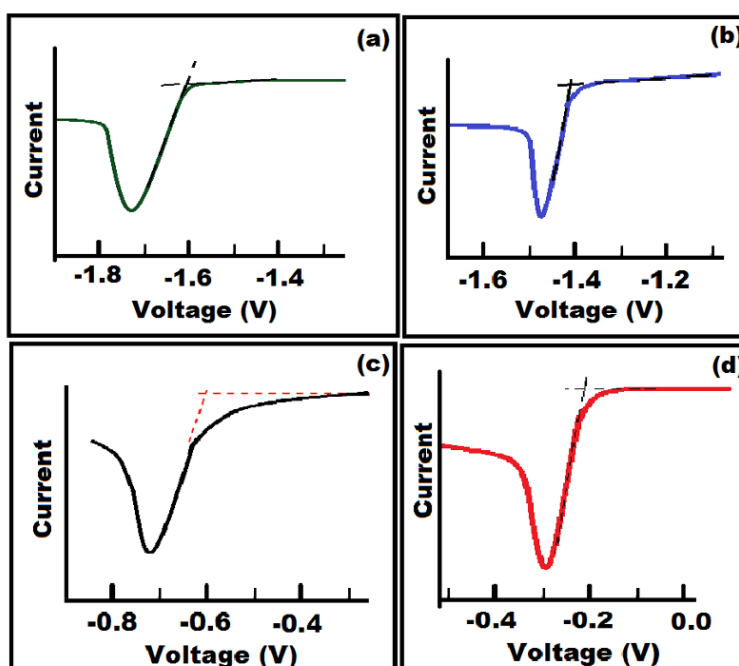
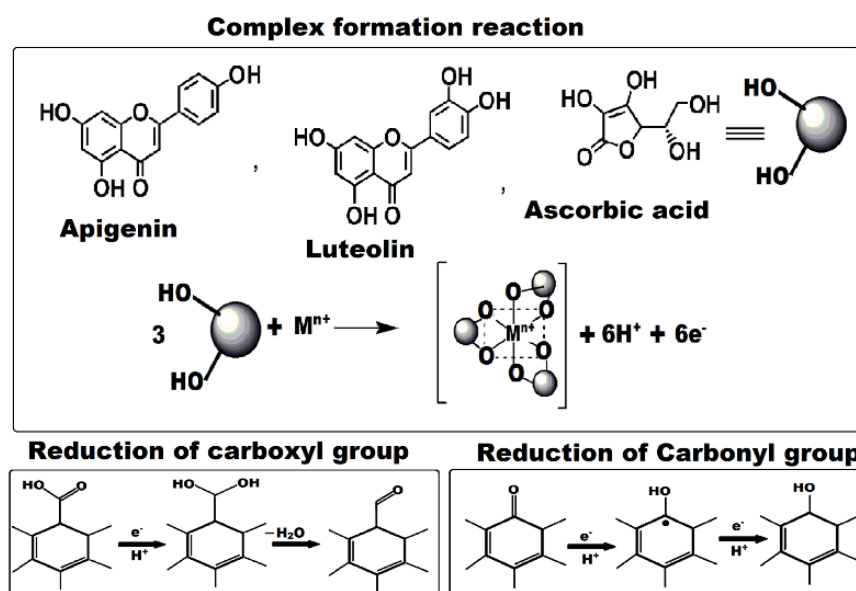


Figure 3A.10 Cyclic voltammograms of (a) *C. esculenta* aqueous extract, (b) *C. esculenta* aqueous extract in the presence of Fe^{3+} ions, GO at pH (c) 6.0 and (d) 3.2

The difference between the reduction potential (ΔE°) of the systems: (i) PP without metal ion was 1.0V (1.6- 0.6V) and (ii) metal ion containing PP was 1.19V (1.4-0.21V), was slightly increased when complexation was taken placed. But this slight increase of ΔE° unable to influence the reduction process. These indicate that high release rate of electron and formation of H^+ have more influence on the reduction. Plausible electron transfer mechanism for the reduction of GO is shown in **Scheme 3A.2**. The reduction was achieved by electron transfer as well as nucleophilic attack (SN^2) mechanism as shown in **Scheme 3A.1**.

The reduction of GO was attained by the sonochemical method. This method is a promising technique as ultrasound irradiation drives some special features such as elevated temperature, high pressure and rapid cooling rates, etc. which are not occurred usually in the ordinary chemical reactions.³⁰ During the ultrasonication, small vacuum cavities are formed in the liquid medium. These cavities rapidly implode and generate microscopic shock waves. This cavitation is extremely powerful especially when the collective energy of all the imploding cavities is combined. Such cavities are formed and collapsed within microseconds and thereby releasing tremendous energy in the liquid medium.¹⁵ Thus, the use of ultrasound irradiation prevents the agglomeration of GO during the reduction which eases more reactions in between the layers of GO. This is really difficult to create in the conventional chemical reaction. In addition to this, the radicals produced in the reaction medium during ultrasonication also play a crucial role in the reduction of GO.³⁰ The removal of oxygen containing groups of GO is facilitated by ultrasound irradiation due to enhance interactions of such groups with H^+ and e^- formed during complexation reaction. In addition to that the effect of extreme temperature, pressure and high cooling rates due to the acoustic cavitation phenomena catalyzes the reduction within a shorter time. Also, it is well known that GO is thermally unstable above 200 °C, the high temperature produced during the ultrasound irradiation itself able to reduce the GO.



Scheme 3A.2 Possible electron transfer reduction mechanism of GO using *C. esculenta* leaf aqueous extract in presence of Fe^{3+} ions

Thus, the ultrafast reduction of GO was achieved by the combined effect of ultrasonication and Fe³⁺ ions in the presence of *C. esculenta* leaf aqueous extract. This may be due to fast complexation of phytochemicals with Fe³⁺ ions and generation of extreme reaction condition by ultrasonication. Hence, the reported approach for the reduction of GO was completed within 3 min.

3A.4. Conclusion

So, the study revealed that phytoextracts exhibited tremendous potential to be used as reducing agents for the reduction of GO by an environmental benign synthetic protocol. The most important advantages of the phytoextracts are their abundance in nature, cost effectiveness and easy product isolation after reduction as they can be extracted from non-edible or waste plant products. The values of specific capacitance, high electrical conductivity and high carbon to oxygen ratio of the prepared RGO are acceptable. Thus, this green method can be used for a large scale production of RGO.